

Improving the Accuracy of Volumetric Segmentation Using Pre-Processing Boundary Detection and Image Reconstruction.

Rick Archibald, Jiuxiang Hu, Anne Gelb, and Gerald Farin

Abstract—The concentration edge detection and Gegenbauer image reconstruction methods were previously shown to improve the quality of segmentation in magnetic resonance imaging. In this study these methods are utilized as a pre-processing step to the Weibull E-SD field segmentation. It is demonstrated that the combination of the concentration edge detection and Gegenbauer reconstruction method improves the accuracy of segmentation for the simulated test data and real magnetic resonance images used in this study.

Index Terms—3D Segmentation, Weibull E-SD field, Edge Detection, Gegenbauer Reconstruction, Magnetic Resonance Imaging.

I. INTRODUCTION

VOLUMETRIC data sets, common in many scientific and medical fields of research, consist of multi-dimensional discrete points in which each point represents a physical parameter in a finite region of space. Typically the data sets are three-dimensional and come from measurements on uniform grids, although in some applications the dimension is increased to include time and may be on non-uniform grids. Of particular interest in the analysis of these types of data sets is the determination of regions that are homogeneous with respect to some characteristic, for instance, intensity or texture. The classification of complete homogeneous regions within volumetric data sets is called segmentation.

The importance of segmentation in the analysis of volumetric data is represented by active and widespread research. Segmentation is routinely used in satellite-based remote sensing technology, which is capable of acquiring volumetric data sets of not only the earth's surface and atmosphere, but also the sun's photosphere. In this situation, segmentation is used to determine features corresponding to geographical landscapes, physical storms [19], sunspots [4], and more. Volumetric data sets of geologic deposits are routinely constructed from seismic data, in which segmentation is performed in order to recognize subsurface structural features from variational characteristics [18]. In medicine, a number of technologies

produce volumetric data sets, which include magnetic resonance (MR), X-ray computed tomography (CT), positron emission tomography (PET), and ultrasound [23]. The amount and importance of the volumetric data sets collected from these different medical modalities have inspired much research in the segmentation of anatomical structures in the human system [5], [8], [21], [25], [26].

Previous work has demonstrated that the Gegenbauer reconstruction method, a high order image reconstruction method first introduced in [15], in combination with the concentration edge detection method, introduced in [11], is an effective pre-processing step in medical segmentation [1]. The purpose of this study is to improve the accuracy of the Weibull E-SD field segmentation method, which was first developed in [16] as an effective coarse-grain approach to volumetric segmentation. This will be accomplished by effectively pre-processing data through the concentration edge detection and Gegenbauer reconstruction methods. The advantage of the Gegenbauer reconstruction method over other types of reconstruction procedures lies in its ability to reconstruct an entire image with exponential accuracy. Its success hinges on the knowledge of the structural edges [14], and hence edge detection is a critical first step. Both the concentration edge detection method [2], [11], [12], and Gegenbauer reconstruction procedure have been shown to be stable and robust in the presence of noise [3], and are therefore well suited for volumetric reconstruction and segmentation.

The fundamental assumption in the Weibull E-SD field segmentation method, [16], is that regions which are homogeneous with respect to some characteristic will have similar local expectation and standard deviation. The ordered pair of local expectation and standard deviation for each point in the volumetric space forms the so-called E-SD field. It has been demonstrated in [6] that the estimation of the E-SD field is not stable in the presence of noise and becomes dependent on the statistical model of the noise. Since noise is inherent in physical situations, it becomes imperative to use an appropriate statistical framework in the modelling of noise in the volumetric data set so that the effects of noise are minimized and the approximation of the E-SD field is stable.

The characteristics of physical noise in volumetric data is dependent upon the particular technology utilized in measurement. Hence physical noise has been modelled by many different distributions, including Rayleigh [9], Gaussian, Gamma, and Poisson [6]. The Weibull distribution, introduced in 1939 by W. Weibull, is inspired by the statistical theory of strength

R. Archibald is with the Center for System Science and Engineering Research (SSERC), Arizona State University, Tempe, AZ 85287. E-mail: archi@math.la.asu.edu.

J. Hu is with the Department of Bioengineering and Partnership for Research in Stereo Modelling (PRISM), Arizona State University, Tempe, AZ 85287. E-mail: hu.jiuxiang@asu.edu.

A. Gelb is with the Department of Mathematics and Statistics, Arizona State University, Tempe, AZ 85287. E-mail: ag@math.la.asu.edu.

G. Farin is with the Department of Computer Science, Arizona State University, Tempe, AZ 85287. E-mail: farin@asu.edu.

materials. It has the ability to approximate all of the above mentioned distributions by various choices of parameters [24], and therefore is a flexible distribution for the modelling of physical noise in volumetric data. The Weibull E-SD field segmentation method, [16], employs the Weibull distribution to model physical noise in segmentation and utilizes the theory of Weibull distributions to denoise estimates of the E-SD field, thereby dramatically improving segmentation [16].

The paper is organized as follows: In section II the concentration edge detection and Gegenbauer reconstruction methods are reviewed. Their effectiveness is demonstrated for a one dimensional reconstruction problem. In section III the Weibull E-SD field segmentation algorithm is discussed. The edge detection and reconstruction algorithms are combined to preprocess the data. The resulting image is then segmented by the Weibull E-SD field segmentation algorithm. The numerical results are displayed in section IV.

II. HIGH RESOLUTION IMAGE RECONSTRUCTION

The Gegenbauer reconstruction method, introduced in [15], is a high order image reconstruction method capable of reconstructing entire images with exponential accuracy. A critical first step in any high resolution reconstruction method is edge detection. In this study, edge detection is achieved by a combination of the concentration edge detection procedure designed in [11] and [12], with the minimization procedure introduced in [2].

The concentration edge detection and Gegenbauer reconstruction methods are briefly outlined below in sections II-A and II-B. For ease of presentation, the concentration edge detection and Gegenbauer reconstruction methods are first presented in one dimension. Common to both presentations is the assumption that an arbitrary piecewise smooth function $f(x)$, considered without loss of generality on the domain $-1 \leq x \leq 1$, is known only on the uniform grid

$$f(x_j), \quad x_j = -1 + \frac{j}{N}, \quad j = 0, \dots, 2N-1, \quad (1)$$

for $N \in \mathbb{N}$. Based on this sampling, the Gegenbauer reconstruction method is capable of approximating $f(x)$ on any smooth interval with exponential accuracy [14]. Thus, if $f(x)$ is piecewise smooth, it is possible to approximate the entire function in each smooth interval with exponential accuracy.

For the sampling in (1), both the concentration edge detection and Gegenbauer reconstruction methods depend upon the discrete Fourier coefficients

$$\tilde{f}_k = \frac{1}{2Nc_k} \sum_{j=0}^{2N-1} f(x_j) e^{-i\pi k x_j}, \quad k = -N, \dots, N, \quad (2)$$

where

$$c_k = \begin{cases} 2, & \text{if } k = \pm N, \\ 1, & \text{otherwise,} \end{cases} \quad (3)$$

which is easily computed using the Fast Fourier Transform (FFT) algorithm. Since both the concentration edge detection and Gegenbauer reconstruction methods employ the FFT algorithm, the speed of computation is of the order of the conventional FFT image reconstruction. The Fourier reconstruction

based on the discrete Fourier coefficients (2) is given by

$$f_N(x) = \sum_{k=-N}^N \tilde{f}_k e^{i\pi k x}, \quad (4)$$

and computed using the Fast Fourier Transform (FFT) algorithm. As an example consider the following piecewise function.

Example 1:

$$f(x) = \begin{cases} -x \sin(\pi x), & \text{if } -1 \leq x \leq 0, \\ x^3 + 1, & \text{if } 0 < x \leq 1. \end{cases} \quad (5)$$

The Fourier reconstruction of the piecewise smooth function (5) leads to spurious oscillations and reduced overall convergence, typically known as the Gibbs phenomenon. Figure 1(b) demonstrates this effect. High resolution reconstruction aims to reduce this effect while maintaining the finer features of the function.

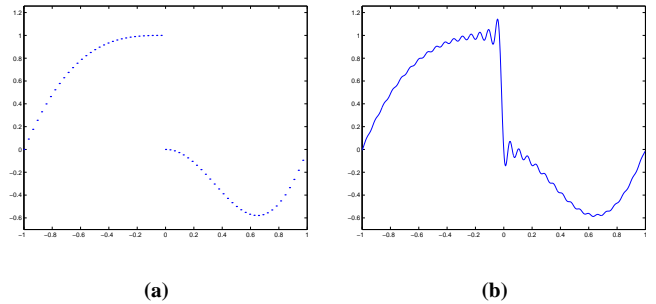


Fig. 1. (a) Sampling of the function (5) on $2N = 64$ uniform grid points. The (b) Fourier reconstruction (4) based on this sampling.

A. Edge Detection

Consider an arbitrary piecewise smooth function $f(x)$. Define the jump function $[f](x) := f(x+) - f(x-)$, where $f(x\pm)$ are the right and left side limits of the function at x , $f(x\pm) = \lim_{x \rightarrow x\pm} f(x)$. Note that $[f](x)$ is zero away from an edge, and is the value of the jump at an edge. In the case of function (5) of example 1 the jump function is

$$[f](x) = \begin{cases} -1, & \text{if } x = 0, \\ 0, & \text{otherwise.} \end{cases} \quad (6)$$

Based on the Fourier coefficients (2), it is shown in [11] that the concentration edge detection method converges to the jump function and is easily implemented as

$$\begin{aligned} T_N^\tau[f](x) &:= i\pi \sum_{k=-N}^N \text{sgn}(k) \tau\left(\frac{|k|}{N + \frac{1}{2}}\right) \tilde{f}_k e^{i\pi k x} \\ &\longrightarrow [f](x), \quad \text{as } N \longrightarrow \infty. \end{aligned} \quad (7)$$

Here $\tau(\xi)$ is called the concentration factor, and is determined in [11] to satisfy

$$\frac{\tau(\xi)}{\sin(\xi\pi)} \in C^2(0, 1),$$

and normalized so that

$$\frac{\pi}{2} \int_0^1 \frac{\tau(\xi)}{\sin(\xi\pi)} d\xi = 1.$$

In [11] it was shown that the concentration factor belongs to a class of functions that accelerate the rate of convergence of the concentration edge detection method (7) to the jump function. The concentration factor used in this study is the exponential concentration factor,

$$\tau(\xi) = \frac{2c \sin(\xi\pi) e^{\frac{1}{\alpha\xi(\xi-1)}}}{\pi}, \quad (8)$$

where

$$c = \int_{\epsilon}^{1-\epsilon} e^{\frac{-1}{\alpha\eta(\eta-1)}} d\eta. \quad (9)$$

This concentration factor is particularly effective, as it takes full advantage of the spectral data by rapidly converging away from the discontinuities. The parameter α is freely chosen, with a typical value $\alpha = 6$.

The concentration edge detection method (7) will have spurious oscillations in the neighborhood of an edge. In order to determine the exact intervals of smoothness, which is imperative for high resolution reconstruction, we adopt a minimization procedure introduced in [2] given by

$$\begin{aligned} \min_{M, a_i, b_i} \max_x |T_N^\tau[h](x)| &:= \min_{M, a_i, b_i} \max_x |T_N^\tau[f](x)| \\ &+ \sum_{i=1}^M \frac{a_i}{2} |T_N^\tau[g](x; b_i)|, \end{aligned} \quad (10)$$

where

$$h(x) := f(x) + \sum_{i=1}^M \frac{a_i}{2} g(x; b_i) \quad (11)$$

and

$$g(x; b_i) = \begin{cases} x + 1, & \text{if } -1 \leq x \leq b_i, \\ x - 1, & \text{if } b_i < x \leq 1. \end{cases} \quad (12)$$

The minimization procedure (10) is based on the function $h(x)$, which will be smooth function if all the discontinuities of $f(x)$ are subtracted through the use of the sawtooth functions (12). If $h(x)$ is a smooth function, $T_N^\tau[h](x) \rightarrow 0$, and therefore the correct minimization of (10) yields the number of discontinuities, M , with the associated positions, b_i , and magnitudes, a_i , for $i = 1, \dots, M$, of the function f .

In order to demonstrate the concentration edge detection method, consider again the piecewise smooth function (5) of example 1. Figure 2(a) depicts the concentration edge detection method (7) of the piecewise smooth function (5). Clearly the concentration edge detection method converges to the jump function (6), but has spurious oscillations in the neighborhood of an edge. Utilizing the minimization method (10), as depicted in figure 2(b), further improves the concentration edge detection method.

The edge detection method and minimization process can be extended to detect the size and position of discontinuities of a multiple dimensional function by holding all but one dimension fixed and determining the edges as a function of

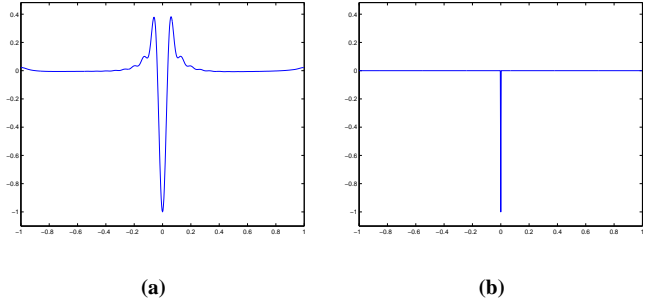


Fig. 2. (a) Concentration edge detection method (7) of the piecewise smooth function (5). (b) Minimization of the concentration edge detection method (10). Here $2N = 64$.

the fixed coordinates. This three dimensional procedure is used for all images processed in this paper. The employment of the FFT algorithm for the edge detection procedure ensures high speed of computation.

B. Gegenbauer Reconstruction Method

The Gegenbauer reconstruction method was developed in [15] and extended in a litany of articles (consult [14] for references). It is a powerful tool that recovers piecewise smooth functions with spectral accuracy up to the edges in each smooth interval without blurring features, hence mitigating the common problem associated with filtering.

The Gegenbauer polynomial $C_n^\lambda(x)$ is an orthogonal polynomial of order n that satisfies

$$\int_{-1}^1 (1-x^2)^{\lambda-\frac{1}{2}} C_k^\lambda(x) C_n^\lambda(x) dx = \begin{cases} h_n^\lambda, & k = n, \\ 0, & k \neq n, \end{cases} \quad (13)$$

where (for $\lambda \geq 0$)

$$h_n^\lambda = \frac{\sqrt{\pi} C_n^\lambda(1) \Gamma(\lambda + \frac{1}{2})}{\Gamma(\lambda)(n + \lambda)}, \quad (14)$$

and

$$C_n^\lambda(1) = \frac{\Gamma(n + 2\lambda)}{n! \Gamma(2\lambda)}. \quad (15)$$

For ease of presentation let us first introduce the Gegenbauer reconstruction method for a one dimensional piecewise smooth function $f(x)$, considered without loss of generality on the domain $-1 \leq x \leq 1$. The Gegenbauer reconstruction method is performed in each smooth interval $[a, b] \subset [-1, 1]$. Since the Gegenbauer polynomials are orthogonal on the interval $[-1, 1]$, a linear transformation from the interval $x \in [a, b]$ to $\eta \in [-1, 1]$ is applied. Specifically, a local variable $\eta \in [-1, 1]$ is defined such that $x(\eta) = \epsilon\eta + \delta \in [a, b]$, where $\epsilon = \frac{b-a}{2}$ and $\delta = \frac{b+a}{2}$. Suppose we are given $f(x_j)$ on equally spaced points as in (1) or equivalently the discrete Fourier coefficients \hat{f}_k in (2). We know that the Fourier partial sum (4) yields a poor approximation to $f(x)$ on $[a, b]$ due to the Gibbs phenomenon. However, information from the Fourier data (2) can still be utilized in the Gegenbauer reconstruction in the following way to approximate $f(x)$ on $[a, b]$:

We define the Gegenbauer reconstruction approximation of $f(x)$ on $[a, b]$ as

$$g_m^\lambda(x(\eta)) = \sum_{l=0}^m \tilde{g}_\epsilon^\lambda(l) C_l^\lambda(\eta), \quad (16)$$

where the approximate Gegenbauer coefficients,

$$\tilde{g}_\epsilon^\lambda(l) = \frac{1}{h_l^\lambda} \int_{-1}^1 (1-\eta^2)^{\lambda-\frac{1}{2}} f_N(x(\eta)) C_l^\lambda(\eta) d\eta, \quad (17)$$

are based on the Fourier approximation of $f(x)$ in $[a, b]$,

$$f_N(x(\eta)) = f_N(\epsilon\eta + \delta) = \sum_{k=-N}^N \tilde{f}_k e^{ik\pi(\epsilon\eta + \delta)}. \quad (18)$$

It is demonstrated in [15] that the approximate Gegenbauer coefficients (16) can be calculated as

$$\tilde{g}_\epsilon^\lambda(l) = \sum_{k=-N}^N \tilde{c}_k^{\lambda, l, \epsilon} e^{ik\pi\delta} \tilde{f}(k), \quad (19)$$

where

$$\tilde{c}_k^{\lambda, l, \epsilon} = \begin{cases} 1, & \text{if } k = 0, \\ \Gamma(\lambda) i^l (l + \lambda) J_{l+\lambda}(\pi k \epsilon) \left(\frac{2}{\pi k \epsilon}\right)^\lambda, & \text{if } k \neq 0, \end{cases} \quad (20)$$

and $J_{l+\lambda}(\pi k \epsilon)$ is the Bessel function of the first kind. Hence the poorly performing Fourier approximation f_N (18) can be changed into a highly accurate Gegenbauer reconstruction (16) of f via the Gegenbauer coefficients (17), or equivalently (20). We note that in practice there may exist some smooth intervals that consist of too few points to construct an approximation. The Gegenbauer reconstruction requires a theoretical minimum of at least π points to form an approximation [13]. Therefore, in intervals containing too few points, the values at each grid point are assumed constant and equivalent to the values determined at the edges by the edge detection method [2].

The parameters m and λ depend upon the number of points, N_I , in the subinterval, $I = [a, b]$, that is reconstructed. A specific requirement is that $m \leq N_I$. Recent work demonstrates how the parameters m and λ can be optimized for a particular subdomain [10]. For simplicity, we choose the parameters such that $\lambda = m$ with

$$m = \max \left\{ 1, \min \left\{ m_{max}, \left\lceil \frac{N_I}{4} \right\rceil \right\} \right\}, \quad (21)$$

where $\lceil x \rceil$ is the minimal integer which is greater than or equal to x , and $m_{max} = 12$.

In order to demonstrate the Gegenbauer reconstruction method, consider again the piecewise smooth function (5) of example 1. Figure 3(a) depicts the Gegenbauer reconstruction method (16) of the piecewise smooth function (5) where it is evident that the Gegenbauer reconstruction not only removes the Gibbs phenomenon, but is also exponentially accurate up to the edges. The accuracy of both the Fourier and Gegenbauer reconstruction methods are depicted in the log-error plot in figure 3(b), where it can be seen that the Gegenbauer reconstruction method is significantly more accurate.

The Gegenbauer reconstruction method can be directly extended to multiple dimensions by performing reconstruction

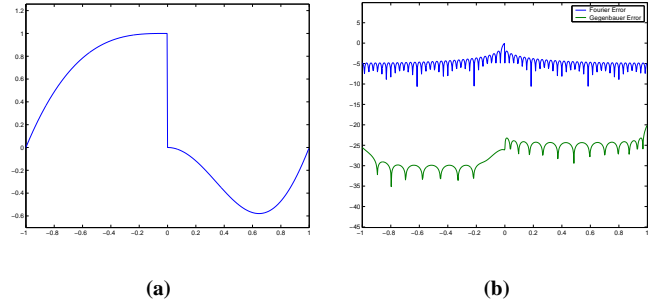


Fig. 3. (a) Gegenbauer reconstruction (16) of the piecewise smooth function (5). Here the Gegenbauer reconstruction parameters are $m = \lambda = 12$. (b) Log-error plot of the Fourier and Gegenbauer reconstruction, with $2N = 64$ pseudo spectral Fourier coefficients.

in smooth regions. The reconstruction will have exponential accuracy up to the edges of each smooth region. Three dimensional Gegenbauer reconstruction is used for all the images processed in this paper. The employment of the FFT algorithm for the Gegenbauer reconstruction procedure ensures high speed of computation.

III. SEGMENTATION

This study employs the Weibull E-SD field volumetric segmentation method, which was first introduced in [16]. For each data point of the discrete volumetric data set the E-SD field consists of an ordered pair representing the local expectation and standard deviation. This segmentation method assumes that homogeneous structures can be characterized by similar local expectancy and variance. Thus, homogeneous structures are contained in a tight region of the E-SD field, enabling segmentation by windowing regions in the E-SD field.

The Weibull E-SD field segmentation method [16] is briefly described below. Section III-A develops the concept of E-SD fields, section III-B introduces the Weibull distribution and the data set noise model, and section III-C describes the denoising procedure.

A. E-SD Fields

In order to preserve continuity with the previous image reconstruction presentation, we model a given volumetric discrete data set as a three-dimensional function $f(x, y, z)$, considered without loss of generality on the domain $-1 \leq x, y, z \leq 1$, sampled on the uniform grid

$$U = \left\{ \left(\frac{2i - N_x}{N_x}, \frac{2j - N_y}{N_y}, \frac{2k - N_z}{N_z} \right) \mid \begin{array}{l} i = 0, \dots, N_x \\ j = 0, \dots, N_y \\ k = 0, \dots, N_z \end{array} \right\}, \quad (22)$$

for $N_x, N_y, N_z \in \mathbb{N}^+$. The local data or κ -voxel, which is a cube of grid points, is defined as

$$\Delta \subset U,$$

such that the dimensions of Δ is $\kappa \times \kappa \times \kappa$.

In order to characterize homogeneous structures within the discrete volumetric data set, it is necessary to define the random variable

$$X_{\Delta}(v) = \#\{(x, y, z) \in \Delta \subset \mathbf{U} | f(x, y, z) = v\}. \quad (23)$$

Thus $X_{\Delta}(v)$ is the number of data points in κ -voxel, $\Delta \subset \mathbf{U}$, which have the value v . The density distribution $d_{\Delta}(v)$ of the random variable $X_{\Delta}(v)$ is defined as

$$d_{\Delta}(v) = \frac{X_{\Delta}(v)}{|\Delta|}. \quad (24)$$

where $|\Delta|$ denotes the number of elements in Δ . In general, the expressions of local expectancy and standard deviation of a κ -voxel are given as follows [7], [17], [22]:

$$E[X_{\Delta}] = \frac{1}{|\Delta|} \sum_{(x,y,z) \in \Delta} f(x, y, z), \quad (25)$$

and

$$SD[X_{\Delta}] = \sqrt{\frac{1}{|\Delta|} \sum_{(x,y,z) \in \Delta} f^2(x, y, z) - E^2[X_{\Delta}]}. \quad (26)$$

Definition 1 describes a spatially distributed object, which is based on the above random variable (23). It is assumed for the Weibull E-SD field volumetric segmentation method that homogeneous structures are spatially distributed objects.

Definition 1: A region Ω is called a spatially distributed object (SDO), if the expectancy (25) and standard deviation (26) for each κ -voxel, $\Delta \in \Omega$, are relatively constant, i.e.,

$$E[X_{\Delta}] \in (e_1, e_2) \quad \text{and} \quad SD[X_{\Delta}] \in (d_1, d_2), \quad (27)$$

where e_1, e_2, d_1 and d_2 denote predefined constants with $e_1 < e_2$ and $d_1 < d_2$. Here X_{Δ} is a random variable as defined in (23).

If noise is present, then (25) and (26) will not give accurate values [7], [20]. It is therefore necessary to model the noise in the data and use denoising procedures in order to stabilize the approximation of the E-SD field.

B. Weibull Distribution

Weibull distribution, first introduced in 1939 by W. Weibull, is defined by the following probability density function (pdf) [24],

$$p(v) = \frac{a}{b} \left(\frac{v - v_0}{b} \right)^{a-1} \exp \left[- \left(\frac{v - v_0}{b} \right)^a \right], \quad (28)$$

where $v \geq v_0$, $a > 0$ is the shape parameter, $b > 0$ is the scale parameter, and v_0 is the shift parameter (the minimum possible value of the random variable). The s -moment of a Weibull distributed random variable X is given by

$$E[X^s] = b^s \Gamma \left(1 + \frac{s}{a} \right), \quad (29)$$

where $\Gamma(x) = \int_0^{\infty} t^{x-1} e^{-t} dt$ is the gamma function.

One particular strength of the Weibull distribution is the number of other distributions that it can approximate [24].

When the shape parameter of the Weibull distribution is given by $a = 1.0$, it approximates the Poisson pdf. When $a = 2.0$ it approximates Rayleigh pdf, and when $a = 3.0$ it approximates Gaussian pdf. The Weibull pdf (28) is depicted in figure 4 for a range of shape parameter values.

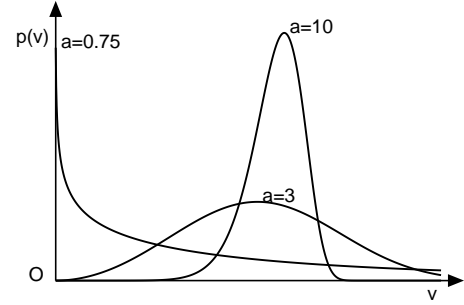


Fig. 4. Weibull Distribution (28) for different shape parameters with $b = 2$ and $v_0 = 0$.

Weibull E-SD field volumetric segmentation method utilizes the Weibull distribution as a model for the physical data noise. This model for noise is local in the sense that the method assumes that each SDO will have constant Weibull distribution parameters.

Finally, it is noted that the approximation of the s -moment for a Weibull distributed random variable is possible by the following property.

Property 1: If X_1, X_2, \dots, X_n are independent identically distributed (iid) random variables with Weibull distribution (28), then

$$\lim_{n \rightarrow \infty} \frac{1}{n} \sum_{i=1}^n X_i = E[X^s], \quad \text{for } 1 \leq s < \infty. \quad (30)$$

C. Weibull Noise Index

As mentioned before, the calculations of (25) and (26) for the E-SD field are not reliable in the presence of noise [7], [20]. However, by modelling the noise with a Weibull distribution, it is possible to use the properties of the Weibull distribution to denoise or improve the signal-to-noise ratio (SNR) in the volumetric data set, and thereby stabilize the approximation of the E-SD field. This section briefly describes the procedure for denoising and stabilizing the approximation of the E-SD field.

Assume that the noise in each SDO of the volumetric data set follows a Weibull distribution with constant parameters. For each κ -voxel, define an auxiliary function $g(s)$ as

$$g(s) = \frac{\left(\sum_{(x,y,z) \in \Delta} f^s(x, y, z) \right)^2}{\kappa^3 \sum_{(x,y,z) \in \Delta} f^{2s}(x, y, z)}, \quad (31)$$

where $s \in (-\infty, \infty)$. As discussed in [16], the auxiliary function is a convex function with maximum at $g(0) = 1$. Using (29) and property 1, the auxiliary function has the following approximation

$$g(s) \approx \frac{(E[X^s])^2}{E[X^{2s}]} = \frac{t_s}{2} B(t_s, t_s), \quad (32)$$

where $t_s = \frac{s}{a}$ and $B(x, y) = \int_0^1 t^{x-1}(1-t)^{y-1}dt$ is the Beta function. Thus, the auxiliary function is dependent on only one Weibull distribution parameter, namely the shape parameter a in (28).

As demonstrated in [16], the auxiliary function (31) is capable of identifying noise in each κ -voxel. Since the maximum of the function $\frac{t_s}{2}B(t_s, t_s)$ is near 0.72, noise may be detected and systematically removed in the κ -voxel by solving the equation $g(s) = 0.72$. The complete Weibull E-SD field volumetric segmentation algorithm, which is presented in [16], is simple and efficient with average complexity of $\mathcal{O}(L \log L)$, where $L := \frac{N_x N_y N_z}{\kappa}$.

IV. NUMERICAL RESULTS

In this section, we will look at two examples illustrating the proposed methods for image reconstruction and segmentation. The first example examines artificial volume data with local Weibull distributed random noise. The second example uses $T2$ weighted MRI scans of a mouse head provided by the Southwest Small Animal Imaging Resource ¹, where the field of view for the MRI scan is $2.56 \times 1.92 \times 1.52$ cm, 100 microns isofield.

A. Controlled Experiment

We validate the use of the concentration edge detection and Gegenbauer reconstruction methods as a pre-processing segmentation step by using simulated volumetric data. The following simple objects are included in the simulated volumetric data; a torus, an ellipsoid, and two deformed cubes. The size of the data set is $100 \times 100 \times 100$ and normalized so that the minimum value is 0 and maximum value is 255. The noise added to every image point has a Weibull distribution and takes the form

$$Y = \min \left\{ 255, C \left[-b \ln(1 - X)^{\frac{1}{a}} \right] \right\},$$

where X is a random variable that is uniformly distributed in $[0, 1]$, the shape parameter a and parameter C are constants within each homogeneous object, i.e.

$$a = \begin{cases} 0.75, & \text{for torus,} \\ 1.2, & \text{for ellipsoid,} \\ 3, & \text{for cubes,} \\ 10, & \text{else,} \end{cases} \quad (33)$$

and

$$C = \begin{cases} 100, & \text{for torus,} \\ 150, & \text{for ellipsoid,} \\ 200, & \text{for cubes,} \\ 250, & \text{else.} \end{cases} \quad (34)$$

The scale parameter b is constant throughout each simulated volumetric data set and incremented as displayed in figure 6. It is noted that the parameter C has the effect of modifying the scale parameter b in each homogeneous object, and thus for this experiment both Weibull distribution parameters can

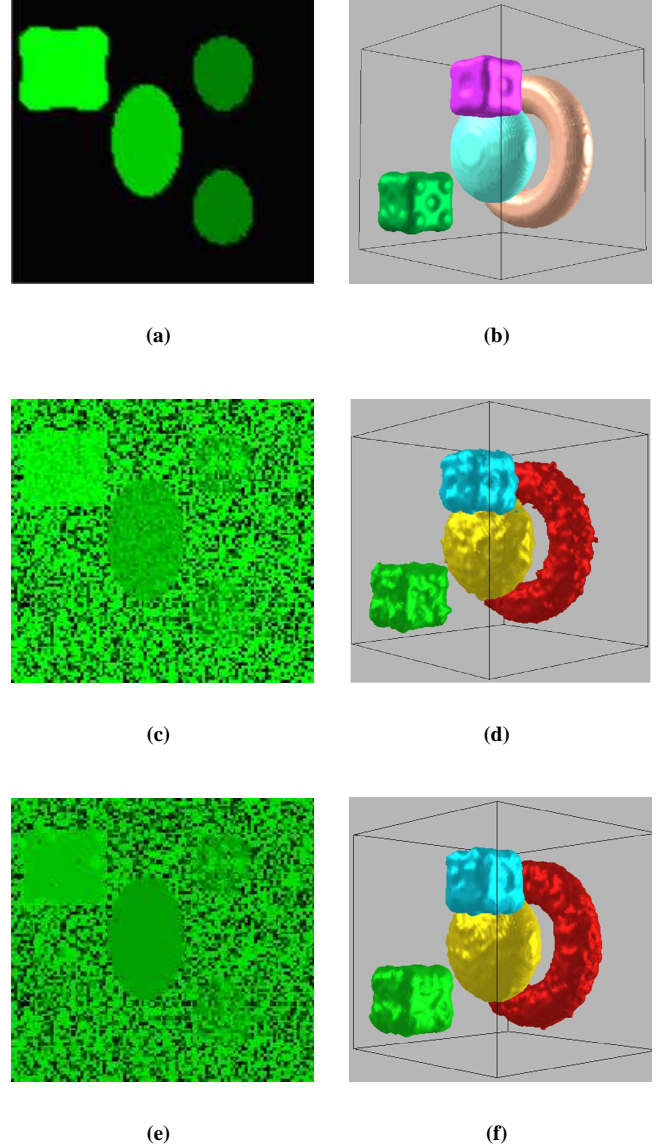


Fig. 5. (a) The slice $(53, y, z)$ of the simulated volumetric data. (b) Reference segmentation. (c) The slice $(53, y, z)$ of the simulated volumetric data with Weibull distributed noise-added data with scale parameter $b = 10$. (d) Segmentation without pre-processing. (e) The slice $(53, y, z)$ of the Gegenbauer reconstruction of the simulated volumetric data. (f) Segmentation with pre-processing.

be considered local parameters with respects to each homogeneous object.

Denote S_n as the support function of the segmentation of any simulated volumetric data set with added noise, and define the support function of the segmentation of the simulated volumetric data set without added noise, denoted as S_r , to be the reference segmentation which is depicted in figure 5(b). A numerical comparison is performed based on segmented volume as measured by the volume deviation (error),

$$\delta(S_r, S_n) = \frac{\sum_{x \in \mathbf{V}} |S_r(x) - S_n(x)|}{\sum_{x \in \mathbf{V}} S_r(x)}. \quad (35)$$

¹Located at the University of Arizona. <http://www.swair.arizona.edu/oct/>

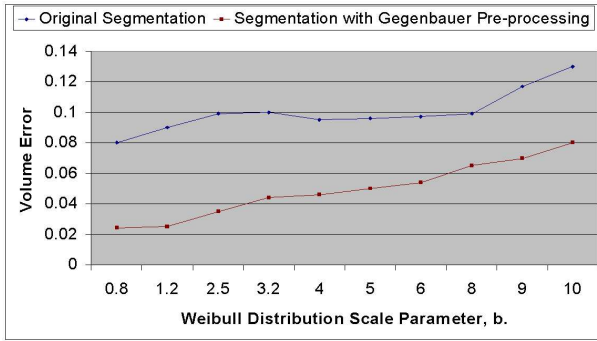


Fig. 6. Volume error (35) in the segmentation of the simulated test data, with and without Gegenbauer pre-processing, for various values of the scale parameter b .

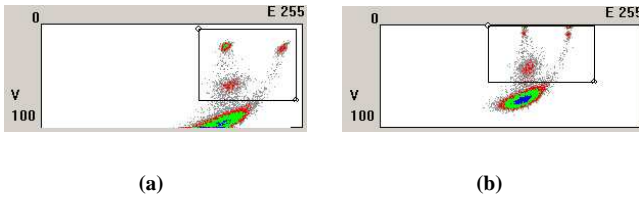


Fig. 7. E-SD fields of the segmented simulated volumetric data (a) without and (b) with Gegenbauer pre-processing. Here the scale parameter for the Weibull distributed noise-added to the data is $b = 10$.

Several levels of noise have been added to the simulated volumetric data to test the concentration edge detection and Gegenbauer reconstruction methods as a segmentation pre-processing step. Depicted in Figure 6 is the volume error, with and without Gegenbauer pre-processing, for various values of the scale parameter b . In every instance, Gegenbauer pre-processing significantly lowers the volume error. Depicted in figures 5(d) and 5(f) are segmentations of the test data, with and without Gegenbauer pre-processing, where the scale parameter of the Weibull noise distribution is $b = 10$. Upon close examination of the surfaces of the segmented test data, it can be observed that the surfaces of the segmented test data with Gegenbauer pre-processing are smoother while the contours and the edges of the original homogeneous objects are preserved.

Also worth noticing is the Weibull E-SD fields of both the original and Gegenbauer pre-processed volumetric data as depicted in figure 7(a) and 7(b). It can be seen that homogeneous objects in the Weibull E-SD field have lower variance and a greater compact representation with Gegenbauer pre-processing. Therefore homogeneous objects are better represented in E-SD field with Gegenbauer pre-processing, which aids in the segmentation process.

B. MRI Data

The segmentation method with Gegenbauer pre-processing is applied to seven different T_2 weighted MRI scans of the heads of mice provided by Southwest Small Animal Imaging Resource. For each scan the field of view is $2.56 \times 1.92 \times 1.52$ cm, 100 microns isofield.

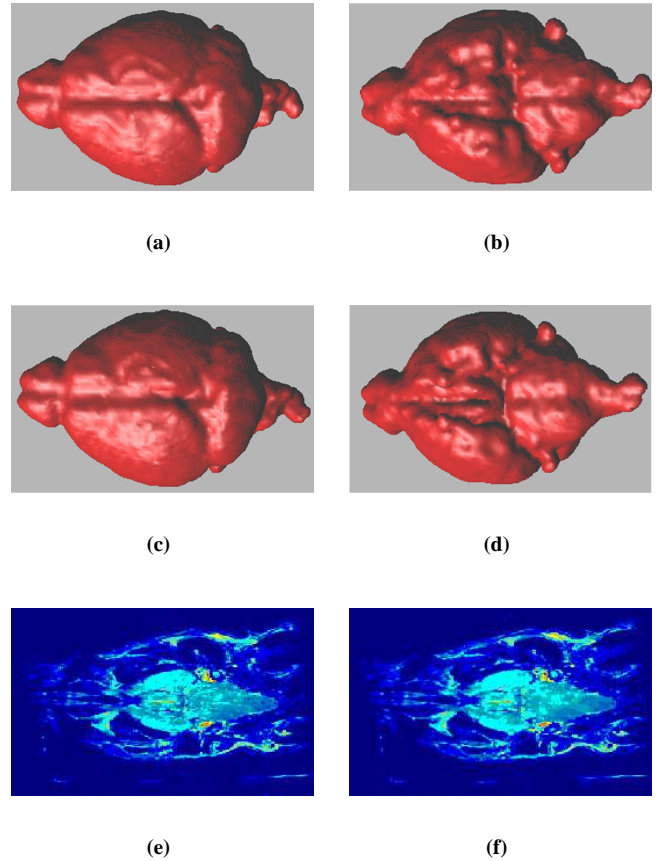


Fig. 8. (a) Top and (b) bottom view of the segmentation of a particular mouse. (c) Top and (d) bottom view of the segmentation of a particular mouse with Gegenbauer pre-processing. (e) The $(x, y, 1.0 \text{ cm})$ cross section of the mouse head data, provided by the Southwest Small Animal Imaging Resource, and (f) the $(x, y, 1.0 \text{ cm})$ cross section of the Gegenbauer reconstructed mouse head data.

Figure 8(a-d) depicts the original and Gegenbauer pre-processed segmentation of one particular MRI scan, where a difference in the surface of the segmented brain is visible. In fact, based on the volume deviation (35), there is an average 8.7% difference between original and Gegenbauer pre-processed segmentation of all seven MRI scans. Upon close examination of the surface of the segmented mouse brain in figure 8(a-d) it can be observed that the surface of the segmented mouse brain with Gegenbauer pre-processing is smoother while the contours and edges are preserved. Features that are noticeably improved through Gegenbauer pre-processing include the shape of the frontal lobe and brain stem. The definition of the contours of the lower brain boundary is another feature that is enhanced through Gegenbauer pre-processing.

Also worth noticing is the E-SD fields of both the original and Gegenbauer pre-processed volumetric data in figure 9, where it is clear that the E-SD field has a greater compact representation of the mouse brain when Gegenbauer reconstruction is used as a pre-processing step. Although difficult to observe in these E-SD fields, there is a reduction of variance when Gegenbauer reconstruction is used as a pre-processing

step. Furthermore, the peak of E-SD field occurs at a variance of 1 when Gegenbauer pre-processing is employed and 3 when it is not. Reduction of variance aids in Weibull E-SD field segmentation.

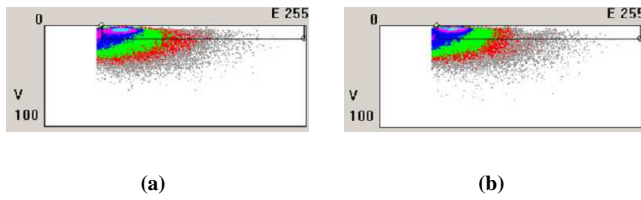


Fig. 9. E-SD Field of segmented mouse (a) without and (b) with Gegenbauer pre-processing.

V. CONCLUDING REMARKS

It has been demonstrated that using the combination of the concentration edge detection and Gegenbauer reconstruction methods as a preprocessing step benefits the Weibull E-SD field segmentation method. The volume error is reduced, the boundaries of segmented homogeneous objects are more accurate, and the representation of homogeneous objects is better constrained in the E-SD field. Additionally, the combination of these methods is a viable approach for segmentation of volumetric data due to their low computational cost and robust nature in the presence of various types of noise.

ACKNOWLEDGMENTS

The work of these authors was supported in part by the Center for System Science and Engineering Research at Arizona State University (R. Archibald and A. Gelb), the Arizona Center for Alzheimer's Disease Research (G. Farin), the US Defense Advanced Research Projects Agency grant No MDA 972-00-1-0027 (J. Hu and G. Farin), NSF grant No DMS01-07428 (A. Gelb), and No IIS-998016 (G. Farin). The authors would like to thank Southwest Small Animal Imaging Resource and PRISM for providing the data and computing resources.

REFERENCES

- [1] R. Archibald, K. Chen, A. Gelb, and R. Renaut, "Improving Tissue Segmentation of Human Brain MRI Through Pre-Processing by the Gegenbauer Reconstruction Method," *NeuroImage*, in press.
- [2] R. Archibald and A. Gelb, "A Method to Reduce the Gibbs Ringing Artifact in MRI Scans While Keeping Tissue Boundary Integrity," *IEEE Transactions of Medical Imaging*, vol. **21**, pp. 305-319, 2002.
- [3] R. Archibald and A. Gelb, "Reducing the effects of noise in boundary detection," *Journal of Scientific Computing*, vol. **17**, pp. 167-180, 2002.
- [4] E. Bratsolis and M. Sigelle, "Solar Image Segmentation by Use of Mean Field Fast Annealing," *Astronomy and Astrophysics Supplement Series*, vol. **131**, pp. 371-375, 1998.
- [5] J. Chen, S. Gunn, M. Nixon, and R. Gunn, "Markov random field models for segmentation of PET images," *Proceedings Information Processing in Medical Imaging*, vol. **2082**, pp. 468-474, 2001.
- [6] C. Chesnaud, P. Refregier, and V. Boulet, "Statistical Region Snake-Based Segmentation Adapted to Different Physical Noise Models," *IEEE Transactions on Pattern Analysis and Machine Intelligence*, vol. **21**, no. **11**, pp. 1145-1157, 1999.

- [7] B. Chanda, B. Chaidhuri, and D. Majumde "A Modified Scheme for Segmenting Noisy Images," *IEEE Transactions on Systems Management and Cybernetics*, vol. **18**, no. **3**, pp. 458-466, 1988.
- [8] A. Dale, B. Fischl, and M. Sereno, "Cortical surface-based analysis. I. Segmentation and surface reconstruction," *NeuroImage*, vol. **9**, pp. 179-194, 1999.
- [9] J. Dias and J. Leitao, "Wall Position and Thickness Estimation from Sequences of Echocardiographic Images," *IEEE Transactions of Medical Imaging*, vol. **15**, no. **1**, pp. 25-38, 1996.
- [10] A. Gelb, "Parameter Optimization and Reduction of Round Off Error for the Gegenbauer Reconstruction Method," to appear in *Journal of Scientific Computing*, 2003.
- [11] A. Gelb and E. Tadmor, "Detection of Edges in Spectral Data," *Applied and Computational Harmonic Analysis*, vol. **7**, pp. 101-135, 1999.
- [12] A. Gelb and E. Tadmor, "Detection of Edges in Spectral Data II. Nonlinear Enhancement," *SIAM J. Numer. Anal.*, vol. **38**, no. **4**, pp. 1389-1408, 2000.
- [13] D. Gottlieb and S. Orszag, *Numerical Analysis of Spectral Methods: Theory and Applications*. SIAM, Philadelphia, 1977.
- [14] D. Gottlieb and C-W. Shu, "On the Gibbs Phenomenon and its Resolution," *SIAM Review*, vol. **39**, pp. 644-668, 1997.
- [15] D. Gottlieb, C-W. Shu, A. Solomonoff, and H. Vandeven, "On the Gibbs Phenomenon I: Recovering Exponential Accuracy From the Fourier Partial Sum of a Nonperiodic Analytic Function," *J. of Comp. and Appl. Math.*, vol. **43**, pp. 81-98, 1992.
- [16] J. Hu, A. Razdan, G. Nielson, G. Farin, D. Baluch, and D. Capco, "Volumetric Segmentation Using Weibull E-SD Fields," *IEEE Transactions on Visualization and Computer Graphics*, vol. **11**, no. **3**, 2003.
- [17] R. Hummel and S. Zucker, "On the Foundations of Relaxation Labeling Processes," *IEEE Transactions on Pattern Analysis and Machine Intelligence*, vol. **5**, no. **3**, pp. 267-287, 1983.
- [18] K. Koester and M. Spann, "Unsupervised Segmentation of 3D and 2D Reflection Data," *International Journal of Pattern Recognition and Artificial Intelligence*, in press.
- [19] V. Lakshmanan, V. DeBrunner, and R. Rabin, "Texture-based segmentation of satellite weather imagery," *Proceedings. 2000 International Conference on Image Processing*, vol. **2**, pp. 732-735, 2000.
- [20] T. Lee, "Segmentation Images Corrupted by Correlated Noise," *IEEE Transactions on Pattern Analysis and Machine Intelligence*, vol. **20**, no. **5**, pp. 481-492, 1998.
- [21] J. Lui, T. Dai, T. Elster, V. Sahgal, R. Brown, and G. Yue, "Simultaneous measurement of human joint force, surface electromyograms, and functional MRI-measured brain activation," *J. Neurosci. Methods*, vol. **101**, pp. 49-57, 2000.
- [22] J. Liu and Y. Tang, "Adaptive Image Segmentation with Distributed Behavior-Based Agents," *IEEE Transactions on Pattern Analysis and Machine Intelligence*, vol. **21**, no. **6**, pp. 544-551, 1999.
- [23] S. Senger, "Visualizing and Segmenting Large Volumetric Data Sets," *IEEE Computer Graphics and Applications*, vol. **19**, no. **3**, pp. 32-37, 1999.
- [24] E. Suhir, *Applied Probability for Engineering and Science*, McGraw-Hill, 1997.
- [25] P. Taylor, Invited Review: "Computer aids for decision-making in diagnostic radiology- a literature review," *Brit.J.Radiol.*, vol. **68**, pp. 945-957, 1995.
- [26] A. Worth, N. Makris, V. Caviness, and D. Kennedy, "Neuro-anatomical segmentation in MRI: technological objectives," *Int.J.Patt.Rec.Art.Intel.*, vol. **111**, pp. 1161-1187, 1997.



Rick Archibald received the BSc degree in honors physics and M.Sc in applied mathematics from University of Alberta, Canada, in 1996 and 1998 respectively. He received the PhD degree in mathematics from Arizona State University in 2002. Presently he is working as a post-doctorate at the Center for System Science and Engineering Research at Arizona State University. His current research interests includes spectral image reconstruction, biological modelling, boundary detection and stochastic problems.



Jiuxiang Hu received the BS, MS, and PhD degrees in mathematics from Huazhong Normal University in 1988, Huazhong University of Science and Technology, Wuhan, China, in 1991, and Lanzhou University, Lanzhou, China in 1994, respectively. He has been an assistant research scientist in the Bioengineering Department and PRISM lab at Arizona State University since 2000. Since receiving the PhD degree, he was a postdoctoral fellow from 1995 to 1996 and then joined the Department of Computer Science, Huazhong University of Science and Technology, where he was promoted to associate professor in 1997. His research interests include computer graphics, visualization, image processing, and expert systems. He has developed and implemented methods to segment biomedical volume data sets, including image statistical modelling and segmentation techniques with application to structural and quantitative analysis of 3D images.



Anne Gelb received the PhD degree in applied mathematics from Brown University in 1996. She was a postdoctoral fellow in the Department of Applied Mathematics at California Institute of Technology from 1996 to 1998. Presently she is an associate professor in the Department of Mathematics and Statistics at Arizona State University. Her interests include solving partial differential equations using higher order methods, including spectral and finite difference methods. In particular, she is interested in constructing methods to adequately handle the development of shock discontinuities in conservation laws. Her recent research focuses on edge detection and image reconstruction techniques, with applications to MRI and PET images.



Gerald Farin received the PhD degree from the University of Braunschweig, Germany, in 1979. He is a professor of computer science at Arizona State University. His interests are curve and surface modelling. He has written several books and other publications on this topic.